Exemplar-Based Radio Map Reconstruction of Missing Areas Using Propagation Priority

Songyang Zhang*, Tianhang Yu*, Jonathan Tivald*, Brian Choi†, Feng Ouyang†, Zhi Ding*, *Fellow, IEEE*
*Department of Electrical and Computer Engineering, University of California, Davis, CA, USA, 95616
†Applied Physics Laboratory, Johns Hopkins University, Laurel, Maryland, USA, 20723
E-mail: {sydzhang, thgyu, jrtivald, zding}@ucdavis.edu, {Brian.Choi, Feng.Ouyang}@jhuapl.edu

***Abstract*—Radio map describes network coverage and is a practically important tool for network planning in modern wireless systems. Generally, radio strength measurements are collected to construct fine-resolution radio maps for analysis. However, certain protected areas are not accessible for measurement due to physical constraints and security considerations, leading to blanked spaces on a radio map. Non-uniformly spaced measurement and uneven observation resolution make it more difficult for radio map estimation and spectrum planning in protected areas. This work explores the distribution of radio spectrum strengths and proposes an exemplar-based approach to reconstruct missing areas on a radio map. Instead of taking generic image processing approaches, we leverage radio propagation models to determine directions of region filling and develop two different schemes to estimate the missing radio signal power. Our test results based on high-fidelity simulation demonstrate efficacy of the proposed methods for radio map reconstruction.**

***Index Terms*—Radio map, inpainting, dictionary learning**

I. Introduction

With increasingly expansion of sensor network and Internet of Things (IoT) deployment, allocation of radio spectrum is becoming more complex and dynamic, and poses further challenges in managing radio resources and enabling new applications [1]. To better capture spectrum usage pattern and improve efficiency o f r esource m anagement, r adio m aps can play more important roles in the modern wireless communication systems. A radio map is generally characterized by the power spectral density (PSD) over geographical locations, frequencies and time [2]. Providing rich and useful information regarding spectrum activities and propagation channels, radio maps can provide information on detailed PSD distribution and help develop spectrum management applications [3]. Usually, a high-resolution radio map should be constructed from sparser measurements [4]. One major challenge lies in reconstructing more complete radio maps from partial observations.

General construction of radio maps utilizes either model-based methods or model-free methods [2]. Model-based methods assume certain signal propagation models to express the received PSD as a combination of transmitted PSD from active transmitters. For example, an interpolation method [5] proposes to utilize log-distance path loss model (LDPL) for Wi-fi radio map reconstruction. In [4], another model-based method introduces the use of thin-plate splines kernels. Different from model-based approaches, model-free methods do not rely on specific signal propagation models but favor neighborhood information. Typical examples include inverse distance weighted (IDW) interpolation [6], Kriging-based interpolation [7] and Radial Basis Functions (RBF) interpolation [8]. In addition, graph-based approaches, such as graph signal processing [9] and label propagation [10], can also assist radio map reconstruction. Beyond interpolation-based methods, machine learning has also attracted significant attention in radio map reconstruction owing to its ability to utilize hidden data features [11]–[13].

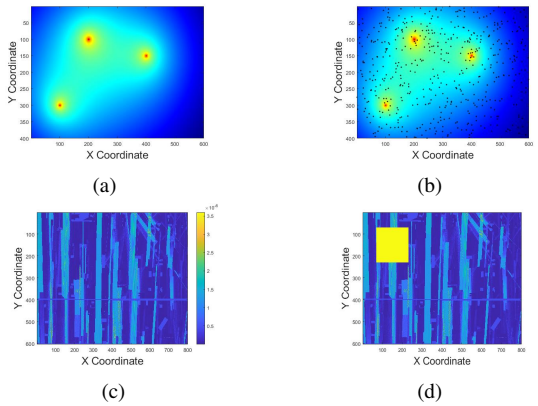

Fig. 1. Examples of Radio Map: Figure (a) and (b) show the power spectrum density and sensor (receiver) placement for general large-scale radio map; Figure (c) and (d) show the spectrum distribution (Watts) and missing observations for restricted areas (marked in yellow) of a small-scale radio map (e.g. several street blocks), which only covers a small part of the large-scale radio map. Note that, the coordinates here are the index of PSD conformed to the grid. Usually, the small-scale radio map has higher resolution and smaller area than the large-scale ones.

Presently, most existing approaches focus on constructing radio maps from sparse observations, where sensors are spread over a given region as shown in Fig. 1(b). However, in cases involving inaccessible, restricted, or protected areas, radio measurement is not available, leading to missing observations of certain regions or blocks. The radio map construction for such restricted areas is more challenging and does not lend themselves to traditional radiomap construction methods.

This work was supported in part by the National Science Foundation under Grant 2029848 and Grant 2002937; and in part by Johns Hopkins University Applied Physics Laboratory Independent Research and Development Funds.

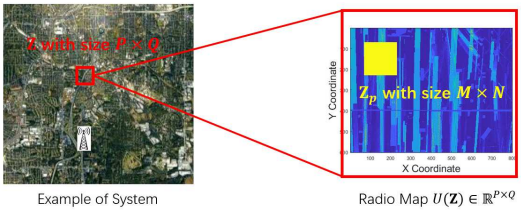

Fig. 2. Illustration of Objective Scenarios: the restricted/inaccessible area $\mathbf{Z}_p$ is marked in yellow with area size $M \times N$ in a small-scale radio map $U(\mathbf{Z}) \in \mathbb{R}^{P \times Q}$.

First, unlike large-scale radio map, missing observations of power spectrum covering restricted areas occur in relatively smaller regions, such as the example of Fig. 1(d). PSD distribution in these small-scale regions tends not to follow well known propagation models but is more sensitive to small scale environmental features, which makes the implementation of model-based methods more difficult. Secondly, since available measurement samples are uneven and observations of some entire segments are missing, interpolation methods are ineffective without accurate and reliable neighborhood information, especially for restricted regions. Last but not least, for practical reasons, observed data are usually limited, providing insufficient training samples for learning-based approaches.

In this work, to capture the spectrum power distribution from limited and uneven observations, we propose an exemplar-based approach using radio propagation priority to reconstruct radio map in restricted or inaccessible areas. The main contributions of our work are summarized as follows:

- Through exploring the pattern of spectrum power from observed data and integrating radio propagation models, we introduce propagation model-based priority to define directions of data filling for missing regions.
- By analyzing correlations from observed signals, we propose to estimate missing radio PSD values based on exemplar copying and dictionary learning, respectively.

We compare our proposed methods with traditional radio map constructions by testing over a Applied Physics Laboratory (APL) dataset from Johns Hopkins University (JHU). Our test results demonstrate the effectiveness of the proposed radio map reconstruction method for restricted/inaccessible areas.

II. Problem Description

Our model considers a wireless network coverage of a rectangular area with one transmitter. All radio observations are arranged on a regular grid and are located in the rectangular area $\mathbf{Z}$ with size $P \times Q$ within the network coverage, denoted by $U(\mathbf{Z}) \in \mathbb{R}^{P \times Q}$ shown as Fig. 2. Here, P and Q are the size of grid. Each observation in $U(\mathbf{Z})$ is characterized by a 2-dimensional (2D) coordinates $Z_i = (X_i, Y_i)$ and the corresponding radio spectrum power $e_i = U(Z_i)$. The restricted/inaccessible area $\mathbf{Z}_p$ with size $M \times N$ is located within $\mathbf{Z}$, marked as yellow in Fig. 2, where $M \leq P, N \leq Q$. No observation within $\mathbf{Z}_p$ is available. Compared to traditional radio map reconstruction problems, the small-scale radio map has higher resolution (e.g., accurate to 1 meter) and smaller area, which make it more sensitive to the nearby environment, such as buildings, trees and roads. Moreover, we only have limited and unbalanced observations around restricted/inaccessible areas. Our goal is to estimate $U(\mathbf{Z}_p)$ in the restricted/inaccessible area $\mathbf{Z}_p$ from other observed samples in area $\mathbf{Z}$.

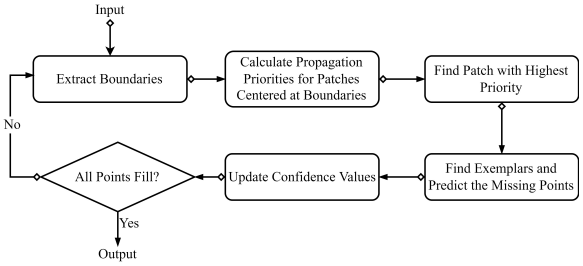

Fig. 3. Scheme of Proposed Method

(a) (b)

Fig. 4. Illustration of Filling Process: a) Select a patch Ψ_q in the boundary $\delta\Omega$; b) Estimate the missing values in Ψ_q and regenerate $\hat{\Psi}_q$

Although we only consider one transmitter here, our framework can be directly extended to multiple transmitters by combining all the transmitted PSD. For convenience, we will focus on the one transmitter case in this work and leave more detailed analysis in future works.

Note that, our objective here is similar to the image inpainting [14] problem in computer vision. However, the traditional image inpainting only concerns about pixel values but not the wireless communication context. Hence, it is ineffective for capturing spectrum power distribution in radio scenarios. Besides observed values, we also consider the radio propagation model to assist radio map reconstruction for restricted/inaccessible areas. More analysis and comparison will be discussed in Section IV.

III. Exemplar-Based Radio Map Reconstruction

In this section, we introduce an exemplar-based radio map reconstruction using radio propagation priority.

A. Overview of the Proposed Method

To fill a region based on surrounding observations, one intuitive way is to estimate the missing values patch (block) by patch (block) from boundaries between observed and target (restricted area) regions to the center of the restricted/inaccessible area. In this work, we follow a similar scheme to reconstruct the radio map from observations as shown in Fig. 3. To estimate radio power in restricted areas, we start from a small selected patch centered at the boundaries shown as Fig. 4. Next, we estimate the missing values for this selected patch and update the boundary. Through patch-by-patch estimation of the missing values, we can obtain the

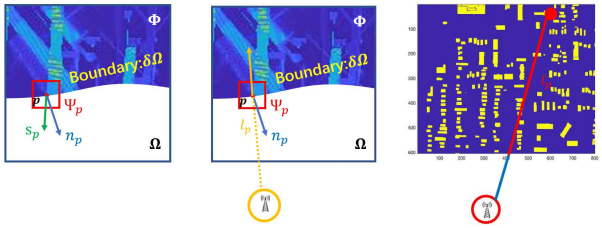

(a) Data term. (b) Radio term. (c) Block term.

Fig. 5. Illustration of Calculating Priority

reconstructed radio map for the whole restricted/inaccessible area. The general steps are described as follows.

- Step 1: Extract the boundary $\delta\Omega$ between observed region Φ and target region Ω (initialized as $\mathbf{Z}_p$) in $\mathbf{Z}$;
- Step 2: Given a patch Ψ_p with size $n \times n$ centered at point p located at boundaries, i.e., $p \in \delta\Omega$, calculate the priority of the patch as $P(p)$ based on the texture properties of observations and radio propagation features;
- Step 3: Order all patches Ψ_p centered at $\delta\Omega$ by $P(p)$ and select the one with highest priority as Ψ_q;
- Step 4: Select exemplars from observed region for Ψ_q and estimate the missing values in Ψ_q;
- Step 5: Update Φ and Ω;
- Step 6: Update the confidence term in the priority;
- Step 7: Repeat Step 1-6 until all the missing values in the restricted/inaccessible area $\mathbf{Z}_p$ are estimated.

From the steps above, the key issues in the proposed method are how to define priority $P(p)$ to determine the filling direction, and how to estimate the missing values from exemplars. We will discuss more details in Section III-B.

B. Details in the Proposed Method

This part introduces definition of priority based on radio propagation and two approaches to estimate the missing radio map values.

1) Definition of Priority: To find a suitable direction of filling the missing region, we expect to propagate the key information in texture and radio spectrum with larger certainty. Thus, we define the priority of patch selection as follows:

$$P(p) = C(p) \cdot D(p) \cdot B(p) \cdot L(p), \tag{1}$$

where the confidence term $C(p)$ together with data term $D(p)$ contain radio map pattern information (texture), whereas radio propagation term $L(p)$ together with block term $B(p)$ describe radio propagation properties. More specifically:

- $C(p)$: The confidence term $C(p)$ describes the confidence level of the PSD within Ψ_p. If there are more points from the observed region, the corresponding patch has a higher confidence value. Suppose that there are $n \times n$ points in Ψ_p. The confidence term is calculated as

$$C(p) = \frac{\sum_{v \in (\Psi_p \cap \Phi)} C(v)}{n \times n}, \tag{2}$$

where $C(v)$ is initialized as $C(v) = 1$ for $v \in \Phi$; otherwise, $C(v) = 0$. For each iteration, confidence term $C(u)$ for a newly-filled point u in $\tilde{\Psi}_q$ is updated by $C(u) = C(q)$ before the next iteration at Step 6.

- $D(p)$: $D(p)$ is the data term describing the gradients of texture. Suppose that the normal of boundary at p is $\mathbf{n}_p$, and the orthogonal direction of the texture gradient at p is $\mathbf{s}_p = \nabla T_p^{\perp}$ where T_p is the power level around p, and $^{\perp}$ is the orthogonal operator. The data term is defined as

$$D(p) = \frac{|\mathbf{s}_p \cdot \mathbf{n}_p|}{\alpha}, \tag{3}$$

where $\cdot$ is the inner product, and α is a normalization factor (e.g., $\alpha = 1$ if $\mathbf{n}_p$ and $\mathbf{s}_p$ are unit vectors). The data term describes the intensity of radio map texture hitting the boundaries.

- $L(p)$: The radio propagation term describes the relationship between the PSD at p and the transmitter at location t. In model-based approaches, signal power is a function of distance to the transmitter [5], [6]. Similarly, we embed the power strength information in $L(p)$ based on the distance $d(t,p)$ between t and p. Since radio propagation property is similar to the texture change described in data term $D(p)$, we can also measure the certainty of radio propagation based on its strengths hitting the boundary:

$$L(p) = |d(t,p)|^{-\beta} |\mathbf{l}_p \cdot \mathbf{n}_p|, \tag{4}$$

where β is the inverse distance parameter, $\mathbf{n}_p$ is the normal of boundary at p and $\mathbf{l}_p$ is the direction of radio propagation from t to p, shown as Fig. 5(b).

- $B(p)$: Since radio map around a restricted/inaccessible area is small-scale and sensitive to the environment, we could also embed information of propagation obstacles in block term $B(p)$. From additional resources, such as satellite image and city map, we can segment buildings (in yellow) and background (in blue) as shown in Fig. 5(c). Let l_p be part of the line connecting t and p within the whole region $\mathbf{Z}$ defined in Section II, i.e., red parts in Fig. 5(c). Then we define $B(p)$ as

$$B(p) = 1 - \frac{\text{the length covering buildings in } l_p}{\text{the total length of } l_p}. \tag{5}$$

If the radio propagates over more obstacles, B_p is smaller and the priority would be reduced.

By selecting those patches with the largest $P(p)$ to fill first, we can determine the filling direction with larger confidence level in both texture and radio propagation. Note that we provide the priority based on single transmitter here. If there are multiple transmitters, one can simply modify $P(p)$ as

$$P(p) = C(p) \cdot D(p) \cdot [\sum_i B_i(p) \cdot L_i(p)], \tag{6}$$

where $B_i(p)$ and $L_i(p)$ are for the ith transmitter. We plan to explore general representations for multiple transmitters in future works.

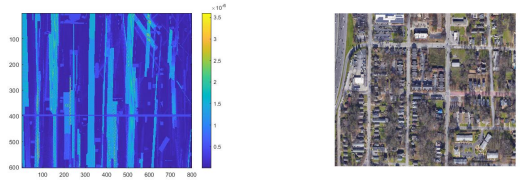

(a) Mean Power (watt). (b) Satellite

Fig. 6. Illustration of APL dataset.

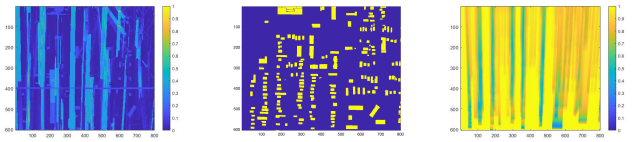

(a) (b) (c)

Fig. 7. Preprocessing of APL Dataset: a) Normalized radio map; b) Segmented buildings; and c) Block term in priority.

2) Estimation of Missing Measurement: After selecting the patch Ψ_q with highest priority, the next step is to estimate the missing measurement values from identified regions. In this part, we introduce two exemplar-based approaches as follows:

- Estimation based on exemplar copy (EPC): Copying values from similar patches in the observed region at the same indices is a widely-used approach to fill the missing regions [16]. Here, we also consider exemplar-based copying to reconstruct the radio map. Let Ψ_q be the $n \times n$ patch selected by $P(p)$. We first find the most similar exemplar patch Ψ_s from the observed region according to

$$\Psi_s = \arg \min_{\Psi_w, w \in \Phi} \sum_{i \in \Phi} [(\Psi_w)_i - (\Psi_q)_i]^2, \tag{7}$$

where $(\Psi)_i$ is the PSD value at position i within the patch Ψ. We then fill the missing value as

$$(\tilde{\Psi}_q)_i = \begin{cases} (\Psi_q)_i & i \in \Phi \\ (\Psi_s)_i & i \in \Omega \end{cases}. \tag{8}$$

- Estimation based on dictionary learning (EPD): Generating a dictionary from observations, one can optimize a sparse vector to combine the code-words in the dictionary to estimate missing values in the patches [17]. After selecting $n \times n$ patch Ψ_q, we can randomly pick W patches from Φ and generate a dictionary $\mathbf{A} \in \mathbb{R}^{n^2 \times K}$ containing K normalized code-words via K-SVD [18] or matching pursuit [19]. Reshaping patch Ψ_q as a vector $\mathbf{x}_q$, we formulate dictionary learning as follows:

$$\tilde{\boldsymbol{\beta}} = \arg \min_{\boldsymbol{\beta}} ||(\mathbf{x}_q)_\Phi - \mathbf{A}_\Phi \boldsymbol{\beta}||_2^2 + \lambda ||\boldsymbol{\beta}||_1, \tag{9}$$

where $\boldsymbol{\beta} \in \mathbb{R}^{K \times 1}$ is a sparse vector and $(\mathbf{x}_q)_\Phi$ is the observed part in Ψ_q. From the optimal $\boldsymbol{\beta}$, we reconstruct the radio map as

$$(\tilde{\Psi}_q)_i = \begin{cases} (\Psi_q)_i & i \in \Phi \\ (\mathbf{A}\boldsymbol{\beta})_i & i \in \Omega \end{cases}. \tag{10}$$

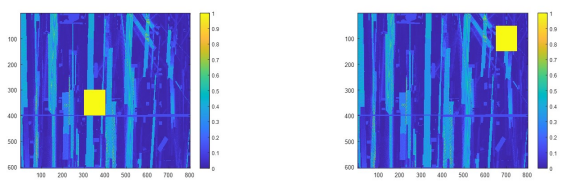

(a) (b)

Fig. 8. Selected Areas to Test Performance: a) Scenario with regular neighborhood pattern; and b) Scenario with complex neighborhood pattern. The restricted/inaccessible areas $\mathbf{Z}_p$ with size 100×100 are marked in yellow.

In general, exemplar-based copying performs better when the radio map has regular, continuous patterns, while the dictionary learning performs better when the environment is more complex. See more discussions in Section IV. Other potential ways to estimate the missing values include subspace learning [20] and graph learning [21].

IV. Experiment Results

In this section, we present test results to demonstrate the efficacy of the proposed methods.

A. Data Information and Preprocessing

Our test is based on the APL dataset which was generated from Wireless inSite Software [15] with Light Detection and Ranging (LIDAR) information of a select region in Atlanta, Georgia, USA. The LIDAR data used for the simulation has a 1-meter resolution. The APL dataset contains a transmitter (Tx) and distributed single-antenna receivers in a 10-block area. The TX antenna is a uniform square array of 16×16 elements, spaced at 0.5 wavelength. The TX is located at latitude/longitude of 33.689/-84.390. The antenna height is 201 meters, and the frequency used is 2660 MHz. The receiver antennas assumed a height of 2.01 meters and uniformly spaced by 0.8 meters. The location of the observed area is at 33.7283∼33.7327 in latitude and -84.3923∼-84.3854 in longitude. To generate the radio map from APL data, we average antenna gains from TX for each data point and conform it to a 604×800 grid, i.e., $U(\mathbf{Z}) \in \mathbb{R}^{604 \times 800}$, where the grid resolution (each 1×1 block) is in 0.8 meters. Note that some original points might be arranged to shared positions in the grid during this process. For those data, the values are further averaged in the shared locations. The mean power in $\mathbf{Z}$, together with its satellite image, are presented in Fig. 6. For convenience, we linearly normalize the radio map between $0 \sim 1$. Note that the original radio map can be transformed without loss from the normalized one, and their pattern are exactly the same shown as Fig. 7(a). Based on the satellite map, we segment the buildings against the background and calculate the block term in the priority by Eq. (5), shown as Fig. 7(b) and Fig. 7(c), respectively.

B. Performance in Selected Areas

To measure performance, we first consider two specific scenarios, i.e., one with regular neighborhood pattern and one with complex neighborhood pattern shown in Fig. 8. In both scenarios, we considered a restricted/inaccessible areas $\mathbf{Z}_p$

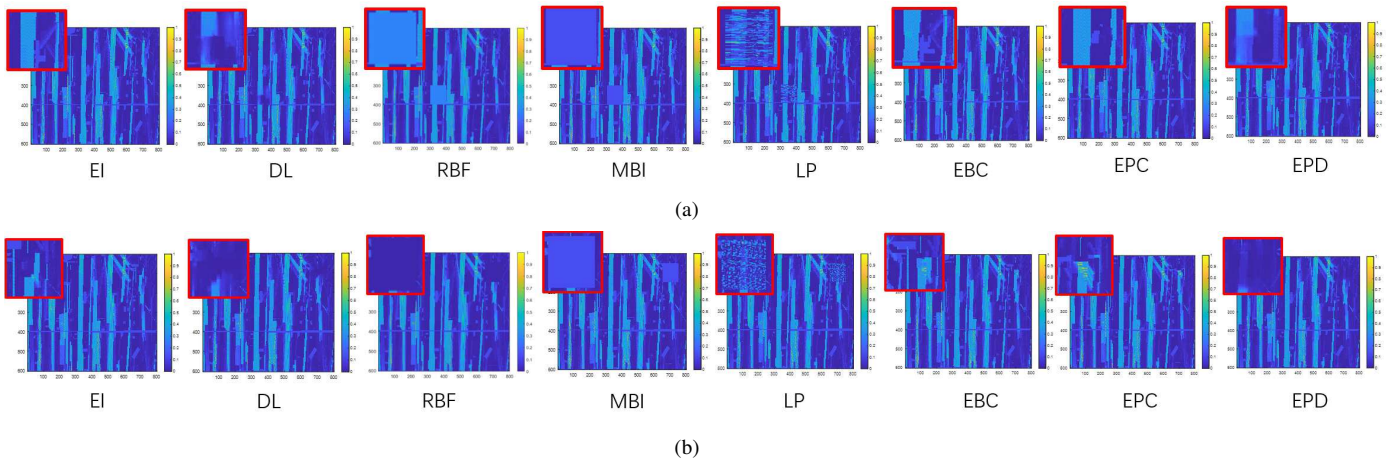

Fig. 9. Visualized Results in Selected Areas: (a) and (b) describe the regular and complex area, respectively; the results in red blocks are zoom-in presentations.

TABLE I
NUMERICAL RESULTS IN SELECTED AREAS.

	EI	DL	RBF	MBI	LP	EBC	EPC	EPD
MSE in Scenario 1	0.0092	0.0152	0.0448	0.0271	0.0327	0.0088	**0.0038**	0.0096
MSE in Scenario 2	0.0258	0.0158	0.0217	0.0173	0.0306	0.0227	0.0152	**0.0136**

with area size 100×100 in grid. The PSD in the whole restricted areas (marked as yellow in Fig 8) is unavailable, which we reconstruct from other observed parts in $\mathbf{Z}$.

We compare our methods with Model-based Interpolation (MBI) [5], Radial Basis Function (RBF) Interpolation [8], Label Propagation (LP) [10], Exemplar-based Inpainting (EI) [16], and Dictionary Learning (DL) [17]. MBI and RBF are interpolation methods based on distances. EI and DL are image inpainting approaches without using radio propagation knowledge. For LP, we incorporate satellite images and information on distance to transmitter as features. For our proposed method, we consider three setups: 1) texture priority together with block term under exemplar-based copy (EBC); 2) complete priority with all 4 terms under exemplar-based copy (EPC); and 3) complete priority with all 4 terms under exemplar-based dictionary learning (EPD). For image inpainting methods and our proposed methods, we select patch size of Ψ_p as 21×21 for fair comparison. For methods related to dictionary learning, we set the number of code-words to $K = 500$. We apply K-SVD [18] to generate the dictionary.

The visualization results are shown in Fig 9, and the corresponding numerical results are shown as Table I. Here, we define MSE $= \frac{1}{m}\sum_{i=1}^{m}(x_i - \tilde{x}_i)^2$, where $\tilde{x}_i, i = 1, \cdots, m$ are the estimated radio map. Shown as Fig. 9, model-based MBI fails to estimate the radio map in the restricted/inaccessible area since the power spectrum in this dataset is over smaller distance variation from the transmitter but is more sensitive to the surrounding environment as seen from Fig. 6. The RBF interpolation also fails to reconstruct missing segments and fills missing radio map with similar values since the observations are uneven, especially near the center of the restricted/inaccessible areas. For learning-based LP, the results display strong noises since the training samples from satellite images are noisy. Compared to the image inpainting methods, the proposed methods based on radio propagation priority show superior performance, since propagation information can enhance the features and textures. As shown in Fig. 7(c), propagation priority terms favor the vertical direction to fill the region, which match the distribution of spectrum pattern in Fig. 6(a). In our proposed methods, copy-based estimations display sharper features while dictionary learning based estimation provides more robust but blurred results. In the first scenario with regular nearby patterns close to the main road, EPC displays significant improvement since the vertical patterns therein is clear and similar. In the second scenario near buildings and trees, EPC sometimes over-estimates some regions from neighborhoods while EPD displays more robustness. The numerical results in Table I are consistent with the visualization results. Thus, one can determine whether EPC or EPD should be selected for estimation depending on the variations of the nearby environment.

C. Overall Performance for Different Area Sizes

We further examine the overall radio map estimation performance for different area sizes. In this test, we compare different methods for restricted/inaccessible areas of various area sizes, i.e., 30×30, 70×70, 100×100, 130×130, and 160×160. For each size, we randomly generate 10 restricted/inaccessible areas as the target region within Fig. 6(a). We then calculate the mean error of different generated areas to implement the comparison. In addition to MSE, we define a normalized error (NE), i.e., NE $= \frac{\sum_{i=1}^{m}(x_i - \tilde{x}_i)^2}{\sum_{i=1}^{m} x_i^2}$. The results are shown in Fig. 10. Since MBI fails to capture the spectrum patterns in small-scale areas, it displays steadily poor result. For other methods, radio map error increases as the area size grows. This is intuitive since neighborhood information and observations become more limited and uneven for larger restricted/inaccessible areas, especially near the center of the

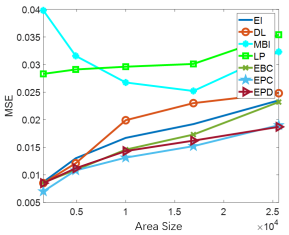

(a) MSE.

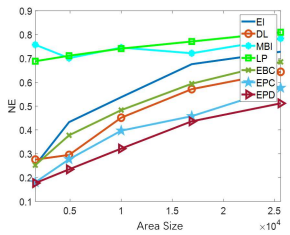

(b) NE

Fig. 10. Numerical Results in Different Area Sizes

TABLE II
MSE IN DIFFERENT PATCH SIZE

Patch Size	9	15	21	27	33
MSE for EPC	0.0177	0.0132	0.0152	0.0163	0.0205
MSE for EPD	0.0020	0.0018	0.0025	0.0027	0.0034

TABLE III
MSE FOR EPD WITH DIFFERENT DICTIONARY SIZE

K (Patch size=15)	500	1000	1500	2000
MSE	0.0026	0.0025	0.0020	0.0020

restricted/inaccessible area. Our proposed methods are better than traditional inpainting and LP approaches, demonstrating the important impact of the proposed radio propagation priority. EPC and EPD show similar MSE results while EPD generate better NE than EPC. The results indicate that EPC works better in some special scenarios whereas EPD is more robust regardless of the power in the restricted/inaccessible areas. The conclusions are similar to Section IV-B and further demonstrate the benefits of the proposed method.

D. Guidelines of Parameter Selection

In this part, we consider the proposed methods under different parameters to develop selection guidelines. We first evaluate the impact of patch sizes in Ψ_p for EPC and EPD in Table. II. For EPC, we test a randomly selected 100×100 restricted/inaccessible area. For EPD, we set $K = 1000$ for the dictionary and test a 40×40 restricted/inaccessible area. Patch size selection is a trade-off between the global information and local observations. For a larger patch size, uncertainty grows with more global information considered. From the results, we determine a suitable patch size around 15$\sim$21. We also test EPD with different dictionary sizes in Table III, which shows that a larger K can achieve better performance.

V. CONCLUSION

In this work, we introduce an exemplar-based approach to wireless radio map reconstruction in the cases of missing measurement. More specifically, we proposed a propagation-based priority to determine the filling direction based on PSD pattern and radio properties. We then introduced two new schemes for patch estimation. The experimental results demonstrate the efficiency of the propagation-based priority to capture the PSD patterns and the power of our proposed method in radio map reconstruction for missing areas, which make further spectrum access and management more reliable for such restricted/inaccessible areas.

REFERENCES

[1] Y. Deng et al., "Radio environment map construction using super-resolution imaging for intelligent transportation systems," in *IEEE Access*, vol. 8, pp. 47272-47281, Mar. 2020.

[2] S. Bi, J. Lyu, Z. Ding and R. Zhang, "Engineering radio maps for wireless resource management," in *IEEE Wireless Communications*, vol. 26, no. 2, pp. 133-141, Apr. 2019.

[3] S. Debroy, S. Bhattacharjee and M. Chatterjee, "Spectrum map and its application in resource management in cognitive radio networks," in *IEEE Transactions on Cognitive Communications and Networking*, vol. 1, no. 4, pp. 406-419, Dec. 2015.

[4] J. A. Bazerque, G. Mateos and G. B. Giannakis, "Group-lasso on splines for spectrum cartography," in *IEEE Transactions on Signal Processing*, vol. 59, no. 10, pp. 4648-4663, Oct. 2011.

[5] M. Lee and D. Han, "Voronoi tessellation based interpolation method for wi-fi radio map construction," in *IEEE Communications Letters*, vol. 16, no. 3, pp. 404-407, Mar. 2012.

[6] S. Kuo and Y. Tseng, "Discriminant minimization search for large-scale rf-based localization systems," in *IEEE Transactions on Mobile Computing*, vol. 10, no. 2, pp. 291-304, Feb. 2011.

[7] G. Boccolini, G. Hernández-Peñaloza and B. Beferull-Lozano, "Wireless sensor network for spectrum cartography based on kriging interpolation," *IEEE 23rd Int. Symp. on Personal, Indoor and Mobile Radio Communications - (PIMRC)*, Sydney, Australia, Sept. 2012, pp. 1565-1570

[8] J. Krumm and J. Platt, "Minimizing calibration effort for an indoor 802.11 device location measurement system,", *Microsoft Research*, Nov., 2003.

[9] A. E. C. Redondi, "Radio map interpolation using graph signal processing," in *IEEE Comm. Letters*, vol. 22, no. 1, pp. 153-156, Jan. 2018.

[10] Y. Ni, J. Chai, Y. Wang, and W. Fang, "A fast radio map construction method merging self-adaptive local linear embedding (lle) and graph-based label propagation in WLAN fingerprint localization systems," *Sensors*, vol. 20, no. 3, p. 767, Jan. 2020.

[11] R. Levie, Ç. Yapar, G. Kutyniok and G. Caire, "Radiouunet: fast radio map estimation with convolutional neural networks," in *IEEE Trans. on Wireless Comm.*, vol. 20, no. 6, pp. 4001-4015, Jun. 2021.

[12] Y. Teganya and D. Romero, "Data-driven spectrum cartography via deep completion autoencoders," in *Proc. ICC-IEEE*, Dublin, Ireland, Jun. 2020, pp. 1–7.

[13] C. Parera, Q. Liao, I. Malanchini, C. Tatino, A. E. C. Redondi, and M. Cesana, "Transfer learning for tilt-dependent radio map prediction," *IEEE Trans. Cognit. Commun. Netw.*, 6(2):829–843, Jun. 2020.

[14] M. Bertalmio, G. Sapiro, V. Caselles, and C. Ballester, "Image inpainting," in *Proc. 27th Conf. on Computer Graphics and Interactive Iechniques*, New York, NY, USA, Jul. 2000, pp. 417-424.

[15] P. Mededovic, M. Veletic and Z. Blagojevic, "Wireless insite software verification via analysis and comparison of simulation and measurement results," in *2012 Proceedings of the 35th International Convention MIPRO*, Opatija, Jul. 2012, pp. 776-781.

[16] A. Criminisi, P. Perez and K. Toyama, "Region filling and object removal by exemplar-based image inpainting," in *IEEE Transactions on Image Processing*, vol. 13, no. 9, pp. 1200-1212, Sept. 2004.

[17] Bin Shen, Wei Hu, Y. Zhang and Y. J. Zhang, "Image inpainting via sparse representation," *2009 IEEE Intl. Conf. on Acoustics, Speech and Signal Processing*, Taipei, May 2009, pp. 697-700.

[18] M. Aharon, M. Elad, and A.M. Bruckstein, "K-svd: design of dictionaries for sparse representation", *Proceedings of SPARSE*, Rennes, France, Nov. 2005, pp.9-12.

[19] S. G. Mallat and Zhifeng Zhang, "Matching pursuits with time-frequency dictionaries," in *IEEE Transactions on Signal Processing*, vol. 41, no. 12, pp. 3397-3415, Dec. 1993.

[20] H. Mobahi, S. R. Rao and Yi Ma, "Data-driven image completion by image patch subspaces," *2009 Picture Coding Symposium*, Chicago, IL, USA, Jul. 2009, pp. 1-4.

[21] Y. Liu and V. Caselles, "Exemplar-based image inpainting using multiscale graph cuts," in *IEEE Transactions on Image Processing*, vol. 22, no. 5, pp. 1699-1711, May 2013.